Letter

Optical telecommunications-band clock based on neutral titanium atoms

Scott Eustice [1,2] Dmytro Filin [3] Jackson Schrott [1,2] Sergey Porsev [3] Charles Cheung [3] Diego Novoa [1,2]
Dan M. Stamper-Kurn [1,2,4] and Marianna S. Safronova [3,5]

[1]*Department of Physics, University of California, Berkeley, California 94720, USA*
[2]*Challenge Institute for Quantum Computation, University of California, Berkeley, California 94720, USA*
[3]*Department of Physics and Astronomy, University of Delaware, Newark, Delaware 19716, USA*
[4]*Materials Science Division, Lawrence Berkeley National Laboratory, Berkeley, California 94720, USA*
[5]*Joint Quantum Institute, National Institute of Standards and Technology and the University of Maryland, College Park, Maryland 20742, USA*

(Received 9 February 2023; accepted 20 April 2023; published 19 May 2023)

We propose an optical clock based on ultranarrow transitions in neutral titanium, which exhibit small blackbody radiation and quadratic Zeeman shifts and have wavelengths in the S-, C-, and L-telecommunications fiber bands, allowing for integration with robust laser technology. We calculate relevant properties using a high-precision relativistic hybrid method that combines configuration interaction and coupled-cluster approaches. To identify magic wavelengths, we have completed the largest-to-date direct dynamical polarizability calculations. Finally, we identify challenges that arise from magnetic dipole-dipole interactions and describe an approach to overcome them. A telecommunications-band atomic frequency standard will aid the deployment of optical clock networks and clock comparisons over long distances.

DOI: 10.1103/PhysRevA.107.L051102

Optical atomic clocks have taken a giant leap in recent years, with several experiments reaching uncertainties at the 10^{-18} level [1–3]. The comparison of clocks based on different atomic standards [4] or placed in separate locations [5] enables important applications such as relativistic geodesy [6], tests of fundamental physics [7], and dark matter searches [8]. These applications motivate the development of synchronized clock networks and transportable clocks that operate in extreme and distant environments [9].

The leading neutral-atom optical clocks operate on wavelengths of 698 nm (Sr) [10] and 578 nm (Yb) [11]. Light at these wavelengths is strongly attenuated in optical fibers, posing a challenge to long-distance time transfer. These wavelengths are also inconvenient for constructing the ultrastable lasers that are an essential component of optical clocks.

By comparison, an optical atomic clock operating in the telecommunication wavelength band would have clear advantages. The S, C, and L bands, ranging altogether between about 1460 and 1625 nm, feature low losses in standard optical fibers. Stable light sources and robust optical amplifiers are also available across these ranges [12]. These features would support the development of fiber-linked terrestrial clock networks over continental distances.

We propose the use of ultranarrow optical transitions in atomic titanium (Ti) as the basis of a telecommunications-band atomic clock. It has recently been pointed out that numerous transition-metal elements, including Ti, can be laser cooled on near-cycling optical transitions [13], allowing for the adoption of optical lattice or tweezer trapping techniques [14] used in today's leading neutral-atom clocks. We identify several transitions between the $3d^24s^2\ a^3F$ and $3d^3(^4F)4s\ a^5F$ fine-structure manifolds in Ti with transition wavelengths between 1483 and 1610 nm (see Fig. 1 and Table I) that can serve as optical clock references for ultrastable telecommunications-band light sources.

From a numerical calculation of the Ti level structure, we identify several key features that make Ti an attractive atom for clock applications: the extreme narrowness of the candidate clock transitions, a weak clock sensitivity to blackbody radiation shifts, and the existence of several magic wavelengths for optical trapping. While we identify challenges posed by the nonzero angular momentum of the clock states in Ti, we show that a proper magic-wavelength condition for optical trapping, which imposes a significant differential tensor ac Stark shift, mitigates their effects.

Our analysis relies on high-precision atomic structure calculations, by which we characterize 85 levels of neutral Ti. For this, we employ a hybrid method that combines the configuration interaction (CI) and linearized coupled-cluster (CC) approaches (referred to as CI+all-order method [15,16]). In this method, the correlations between four valence electrons are included via a large-scale CI computation using a highly parallel message passing interface (MPI) CI code [16,17]. Several computations with increased numbers of configurations were carried out to ensure convergence. The core-core and core-valence correlations are included using an effective Hamiltonian formalism [15]. We construct the effective Hamiltonian using second-order many-body perturbation theory (MBPT) and more accurate CC methods. The difference between these results gives the size of the higher-order corrections, which we use to estimate uncertainties on all theory values [16]. The results are used to calculate transition rates, dynamical polarizabilities, and systematic shifts in the clock transitions. Further details of the computational methods are given in the Supplemental Material [18].

Several clock transitions are identified in Table I. Transitions between the a^3F and a^5F manifolds occur via spin

TABLE I. List of proposed optical clock transitions in Ti. All transitions are between the lower a^3F and upper a^5F terms. The lower (upper) states are indexed by J (J'). Transition wavelengths λ are taken from Ref. [19]. The telecommunications band is indicated, with S (short), C (conventional), and L (long) bands noted. $M1, E2$ reduced matrix elements D_{M1}, D_{E2} and transition linewidths Γ are calculated. The two clock transitions highlighted in the text are in bold.

J	J'	λ (nm)	Tele. band	D_{M1} ($10^{-3}\mu_B$)	D_{E2} (a.u.)	Γ (10^{-6} s^{-1})
4	**5**	**1548.926**	**C**	**1.0(5)**	**0.140(4)**	**242(5)**
4	**4**	**1573.346**	**L**	**0.36(18)**	**0.134(8)**	**239(5)**
4	3	1593.846	L	1.02(12)	0.0015(3)	227(5)
4	2	1609.816	L	N/A	0.0314(27)	214(5)
3	5	1498.615	S	N/A	0.0472(7)	162.2(2.6)
3	4	1521.463	S	0.4(4)	0.027(10)	159.1(2.5)
3	3	1540.625	C	0.2(2)	0.124(4)	147.2(2.6)
3	2	1555.541	C	0.3(4)	0.0204(22)	134.3(2.6)
3	1	1565.754	L	N/A	0.0463(23)	129.2(2.5)
2	4	1483.073	S	N/A	0.0196(26)	32.75(29)
2	3	1501.275	S	0.40(16)	0.024(7)	20.83(36)
2	2	1515.435	S	0.1(1)	0.1006(24)	7.93(38)
2	1	1525.127	S	0.23(2)	0.0643(11)	2.85(11)

forbidden electric quadrupole ($E2$) and magnetic dipole ($M1$) transitions. Calculated reduced matrix elements for these transitions are tabulated. The calculated natural linewidths account for both the decay of the upper state to the lower manifold on the listed $E2$ and $M1$ transitions and the $M1$ decays within each fine-structure manifold. The transitions are all exceptionally narrow, allowing for optical atomic clocks with long coherence times.

In this Letter, we focus on the $a^3F_4 \rightarrow a^5F_5$ transition at 1549 nm unless otherwise noted. An advantage of this transition is that the a^5F_5 state is the lower level of the near-cycling 498 nm transition, which is suited for laser cooling. Our calculations predict that the cooling transition has low branching ratios to other even-parity states ($\sim 10^{-6}$), enabling single-laser state preparation and readout for atoms in the upper clock state. For details on calculations relevant to the laser cooling transition, see the Supplemental Material [18]. An additional benefit is that light at the 1549 nm clock wavelength can be generated by narrow-linewidth, high-power Er-doped fiber lasers, simplifying the required optical setup.

We consider the three titanium isotopes which have zero nuclear spin, and therefore no hyperfine structure (^{46,48,50}Ti). To make the clock insensitive to first-order differential Zeeman shifts from stray magnetic fields, we drive the $|m_J = 0\rangle \rightarrow |m'_J = 0\rangle$ transition, with m_J being the magnetic quantum number and the primed symbols and numbers referring to the upper a^5F state. Because the $E2$ matrix element for this transition is zero, only the $M1$ matrix element contributes to a direct one-photon drive of the clock transition. Choosing quantization, clock-laser polarization, and clock-laser propagation axes as shown in Fig. 1, we calculate that for a driving intensity of 0.1 W/mm^2, we achieve a clock Rabi frequency of 91(46) Hz.

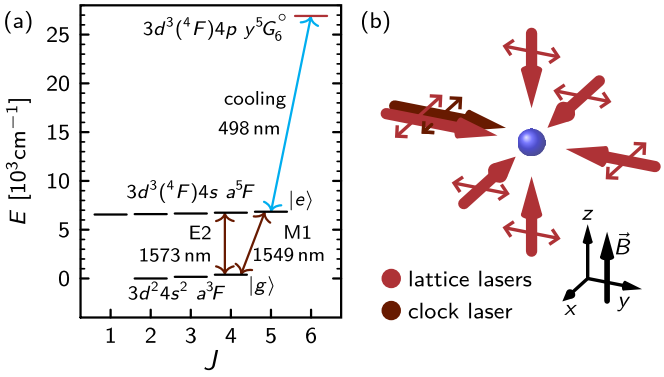

FIG. 1. (a) Relevant atomic structure in Ti for an optical clock. The a^3F and a^5F terms serve as the basis for the optical clock, while the excited $y^5G_6^o$ level serves as the excited state for laser cooling of Ti. The two optical clock transitions highlighted in the text are shown as maroon arrows; the laser cooling transition is shown in cyan. (b) A diagram of the proposed experimental system. Polarizations are indicated on a given beam by a small arrow of the same color as the beam itself.

To compare the strength of this $M1$ transition to that of an $E2$ transition in the same set of transitions, we also consider driving the $|a^3F_4, m_J = 0\rangle \rightarrow |a^5F_4, m'_J = 0\rangle$ transition at a wavelength of 1573 nm. For this transition, the $M1$ matrix element vanishes while the $E2$ matrix element does not. With the same intensity and polarization as in Fig. 1, but propagating along the z axis, the Rabi frequency for such an $E2$ transition is 214(13) Hz. For a detailed derivation of these Rabi frequencies, see the Supplemental Material [18].

Neutral-atom optical clocks often use optical lattice potentials to confine atoms, allowing for a long interrogation time. In order to avoid imposing large differential ac Stark shifts between the upper and lower states of the clock transition, it is necessary to use lattice light which is at a "magic wavelength," at which the dynamic polarizabilities of the lower and upper clock states are identical [20]. In Fig. 2 and Table II, we report several magic wavelengths for the $|a^3F_4, m_J = 0\rangle \rightarrow |a^5F_5, m'_J = 0\rangle$ clock transition. As with most states in Ti, the clock states experience significant vector and tensor ac Stark shifts [13], owing to their nonzero angular momentum and Ti's complex spectrum. To account for these shifts, we

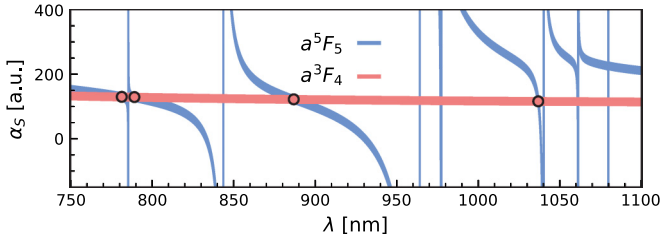

FIG. 2. The scalar dynamic polarizability of the $m_J = 0$ sublevels of the a^3F_4 (red) and a^5F_5 (blue) states in Ti from 1100 to 750 nm as calculated by the sum-over-states method. The angle between the polarization and the B field direction is set to 90°. The locations of magic wavelengths considered in the rest of this work are circled.

TABLE II. Data for the magic wavelengths for the a^3F_4 to a^5F_5 clock transition. Wavelengths are given in units of nm, and polarizabilities are given in atomic units.

λ_{magic}	α	$\alpha^S_{a^3F_4}$	$\alpha^S_{a^5F_5}$	$\alpha^V_{a^3F_4}$	$\alpha^V_{a^5F_5}$	$\alpha^T_{a^3F_4}$	$\alpha^T_{a^5F_5}$
$1036.6^{+0.4}_{-0.4}$	116(10)	115(3)	66(12)	−2(2)	−470(30)	4(4)	154(8)
887^{+4}_{-4}	122(5)	121(4)	159.3(2.6)	−3(2)	−104(5)	5(4)	−111(3)
$789^{+5}_{-2.2}$	129(5)	127(4)	127.1(1.4)	−4(3)	127(4)	5(4)	6.5(1.6)
781^{+3}_{-7}	130(5)	128(4)	126.3(1.3)	−4(3)	138(3)	6(4)	11.5(1.5)

consider the specific lattice configuration shown in Fig. 1. Here, a magnetic field applied in the z direction imposes a linear Zeeman shift and defines the quantization direction. All lattice light is linearly polarized in the transverse x-y plane. In this configuration, the clock transition is shifted only by the differential scalar and tensor ac Stark effects (the vector shift is zero on the $m_J = m'_J = 0$ sublevels). The sum of the scalar and tensor dynamic polarizabilities (α_i^S and α_i^T, respectively) on the transition is then given by

$$\Delta\alpha = \alpha^S_{a^5F_5} - \alpha^S_{a^3F_4} + \frac{1}{2}\left(\frac{2}{3}\alpha^T_{a^5F_5} - \frac{5}{7}\alpha^T_{a^3F_4}\right). \quad (1)$$

At the identified magic wavelengths, the net transition ac Stark shift is zero. For a more detailed description of the ac Stark shifts, see the Supplemental Material [18].

Calculations of the polarizabilities were performed by two methods. First, the sum-over-states method was used to roughly calculate polarizabilities over a wide range of frequencies. The 76 transitions with the largest contributions to dc polarizability were used in the case of the a^3F_4 states, while 51 transitions were used in the case of the a^5F_5 states. Once promising candidates for magic wavelengths were found, we performed direct dynamical polarizability calculations to identify the location of the magic wavelengths more precisely. Direct computations for two of the magic wavelengths allow us to predict the remaining values accurately. Previously, the direct computation method was only used for divalent systems such as Sr [21,22], Mg [23], Yb [24,25], Cd [26], or Tm [27].

For more complex atoms, the rapidly increasing number of relevant configurations makes such a direct computation intractable. Here, we apply instead a truncation approximation: We order the configurations by weight to select the most important ones and then start removing configurations while checking the accuracy of the energies and relevant matrix elements. This procedure drastically reduces the number of Slater determinants required to maintain numerical accuracy. Further details on our method are found in the Supplemental Material [18]. We emphasize that our approach is not specific to Ti; it should allow for the computation of polarizabilities, magic wavelengths, and other atomic properties for other atoms with a complex electronic structure.

Using the lattice configuration and magic wavelength described above not only eliminates the differential light shift, but also protects against the effects of dipole-dipole interactions between Ti atoms. These effects are not present in lattice clocks of Sr, Yb, or Hg as those clocks operate on transitions between nonmagnetic $J = 0$ states. In contrast, the magnetic moments of the proposed Ti clock states are both large, with $\mu_{a^3F_4} = 5.00\mu_B$ and $\mu_{a^5F_5} = 7.05\mu_B$.

There are three processes associated with the dipole-dipole interaction that we consider: dipolar relaxation, elastic spin-spin energy shifts, and inelastic spin-spin mixing [28]. Dipolar relaxation is the process by which Zeeman energy is converted to kinetic energy, depleting atoms from the clock states. Such relaxation can be suppressed for atoms trapped in a deep three-dimensional (3D) optical lattice by ensuring the band gap far exceeds the Zeeman energy [29]. The band energy scale in a lattice is set by the lattice recoil energy $E_r = h^2/(8ma^2)$, where a is the lattice spacing. For a ^{48}Ti atom in the magic-wavelength lattice described above, the recoil energy is $E_r = h \times 6.8$ kHz. 3D optical lattice clocks typically use deep lattices to suppress tunneling and atom-atom contact interactions. As of 2019, the fermionic Sr 3D lattice clock at JILA operated at a lattice depth of $V_0 = 80E_r$ [30]. In deep lattices, the gap above the ground band is $E_g \approx 2\sqrt{V_0 E_r}$. In the case of Ti, a comparable lattice operating at the magic wavelength near 781 nm could be achieved by intersecting six 3.5 W beams with waists of 0.1 mm. This would give a lattice depth of $V_0 \approx 79E_r = h \times 540$ kHz and band gap of $E_g \approx 18E_r = h \times 120$ kHz. Setting the Zeeman energy below this band gap requires the ambient magnetic field be well below $B \sim E_g/\mu_B = 60$ mG.

The second two processes associated with the dipole-dipole interaction are captured in the so-called secular Hamiltonian, which is obtained by time-averaging the dipole-dipole interaction over a Larmor precession:

$$H_{dd} = \frac{\mu_0\mu_B^2}{8\pi}\sum_{\langle i,j\rangle}\frac{g_{J_i}g_{J_j}}{r_{ij}^3}(1-3\cos^2\theta_{ij}) \times\left(J_i^z J_j^z - \frac{1}{4}(J_i^+ J_j^- + J_i^- J_j^+)\right). \quad (2)$$

Here, i and j label two atoms held at different sites of a lattice, separated by a distance vector of length r_{ij} and polar angle θ_{ij} with respect to the quantization axis. g_{J_i} is the Landé g factor of the atom at lattice site i.

The elastic spin-spin energy shift corresponds to the $J_i^z J_j^z$ term in the secular Hamiltonian. In theory, this term generates shifts to the transition frequency between atomic states with nonzero angular momenta. However, for a clock transition between $m_J = m'_J = 0$ magnetic sublevels, the shift is zero and can be ignored.

The final process is the spin-mixing interaction, which corresponds to the $J_i^+ J_j^- + J_i^- J_j^+$ term in the Hamiltonian. This term couples atoms in an initial two-body state $|m_J^{(1)} = 0, m_J^{(2)} = 0\rangle$ to final states $|m_J^{(1)} = \pm n, m_J^{(2)} = \mp n\rangle$, $n \in \{1, \ldots, J\}$. If not controlled, this would lead to a rapid loss of population from the $m_J = 0$ clock states. The

maximal strength of the coupling is $\hbar\Omega_{\rm SM} = \mu_0\mu_B^2 g_J^2 J(J+1)\sqrt{2}/16\pi(\lambda/2)^3$. In a $\lambda = 781$ nm optical lattice, this gives spin mixing strengths of $h \times 2.4$ Hz (4.6 Hz) within the lower (upper) clock state manifold. Spin mixing between atoms in the upper and lower clock states is energetically suppressed because of the significant differential Zeeman splitting. For a 30 mG magnetic field, the splitting between the $|m_J^{(1)} = 0, m_J'^{(2)} = 0\rangle$ and $|m_J^{(1)} = \pm 1, m_J'^{(2)} = \mp 1\rangle$ states is $h \times 6.7$ kHz.

In the case where both atoms occupy either the upper or lower clock state, spin mixing is suppressed by the tensor ac Stark shift imparted by the optical lattice light. The tensor light shift creates an energy splitting between the $|m_J^{(1)} = 0, m_J^{(2)} = 0\rangle$ and $|m_J^{(1)} = \pm n, m_J^{(2)} = \mp n\rangle$ two-atom states. Using the same optical lattice configuration described above, the splitting between the $|m_J^{(1)} = 0, m_J^{(2)} = 0\rangle$ and $|m_J^{(1)} = \pm 1, m_J^{(2)} = \mp 1\rangle$ states is $\Delta E_{\rm tens} = h \times 4(2)$ kHz [$h \times 4.8(6)$ kHz] within the lower (upper) clock state manifold. Since the differential Zeeman splitting and $\Delta E_{\rm tens}$ are much larger than $\hbar\Omega_{\rm SM}$, spin mixing is highly suppressed.

In this regime, spin mixing enters as a second-order perturbative effect. The $|m_J^{(1)} = 0, m_J^{(2)} = 0\rangle$ two-atom states in both the lower and upper clock manifolds are weakly coupled to the corresponding $|m_J^{(1)} = \pm 1, m_J^{(2)} = \mp 1\rangle$ states by $\Omega_{\rm SM}$. Both clock states experience an energy shift on the order of $\sim\Omega_{\rm SM}^2/\Delta E_{\rm tens}$. The difference between the shifts leads to a shift of the clock frequency, while the sum of the shifts leads to decoherence between the clock states. For two atoms, the shift is $\sim$3 mHz and the rate of decoherence is $\sim$6 mHz. For more discussion of the dipole-dipole interaction, see the Supplemental Material [18].

One complication in our scheme of using tensor light shifts to combat magnetic dipole-dipole interactions is that deviations from the lattice-light polarization shown in Fig. 1 will introduce clock frequency shifts. Considering the example parameters from above, a 0.5° tilt of the linear polarization away from the desired orientation would introduce a $\sim$4 Hz overall shift in the clock transition frequency, and a much smaller differential shift spatially across the lattice owing to a variation in the light intensity of the Gaussian-focused beams. Standard methods for reducing and calibrating this residual shift, including measuring the variation of the clock frequency with lattice-light intensity, should allow the systematic uncertainty to be reduced to an acceptable level [30,31].

Additional terms in the light shift, such as the hyperpolarizability and the $M1$ and $E2$ polarizabilities would also need to be taken into account, but their effects are small (below 10^{-18} levels in Sr [32–34]), and their consideration is beyond the scope of this Letter.

Another significant systematic uncertainty in optical clocks is the blackbody radiation (BBR) shift, which has been the subject of significant past investigation [21,35]. We model the BBR shift for the Ti clock line as

$$\Delta_{\rm BBR} = -\kappa\left(\alpha^0_{a^5F_5} - \alpha^0_{a^3F_4}\right)\left(\frac{T}{300}\right)^4(1+\eta), \qquad (3)$$

where $\kappa = \frac{1}{2}(831.9[\text{V/m}])^2$ is a constant of proportionality, α_i^0 is the dc scalar polarizability of the i state of Ti, T is the thermal background temperature measured in K, and η is a small dynamical correction omitted in the present work. The same CI+all-order approach is used to compute dc and dynamic polarizabilities. In this case, we find that $\alpha^0_{a^5F_5} = 128.53$ a.u. and $\alpha^0_{a^3F_4} = 100.39$ a.u., which leads to $\Delta_{\rm BBR} = -0.24$ Hz at $T = 300$ K. This value is approximately an order of magnitude lower than that in Sr, where the BBR shift is known to be -2.2789 Hz [36].

The final systematic uncertainty that we consider is the quadratic Zeeman shift (QZS). For the ^{46,48,50}Ti isotopes, the effect will be small since it will arise only from the mixing of neighboring fine-structure states, whereas in atoms with nonzero nuclear spin, a stronger QZS arises from the mixing of hyperfine states. For the states in the Ti clock, the QZS of the $m_J = 0$ sublevels are $\Delta^{(a^3F_4)}_{\rm QZS} = 0.129[\text{Hz/G}^2]B^2$ and $\Delta^{(a^5F_5)}_{\rm QZS} = 0.434[\text{Hz/G}^2]B^2$, and the QZS on the transition is thus $\Delta_{\rm QZS} = 0.305[\text{Hz/G}^2]B^2$. Given that a Ti clock must operate at a magnetic field well below 60 mG to suppress dipolar relaxation, the QZS of the clock transition will be below 1 mHz. This is approximately an order of magnitude lower than the QZS that is present in Sr optical lattice clocks, of almost 10 mHz [30,31].

Altogether, we have shown that laser-cooled Ti is an attractive choice for realizing a telecommunications-band optical atomic clock. Operating Ti clocks on several of the available telecommunications-band optical transitions would allow for clock comparisons as a powerful method for identifying and reducing systematic corrections. We have advanced atomic structure calculations to determine the critical properties of such clocks, including identifying magic wavelengths for optical trapping, estimating clock transition widths and line strengths, and determining that the BBR shift for Ti clock transitions is an order of magnitude smaller than the shift that dominates current Sr-based clock systematics [30,31]. We also describe potential effects of, and mitigation measures against, magnetic dipole-dipole interactions. These measures are relevant to other potential applications of dipole-interacting atoms and molecules for precision measurement.

We thank M. Kozlov, A. Bondarev, and I. Tupitsyn for helpful discussions of polarizability computations. This work is supported by a collaboration between the U.S. DOE and other Agencies. This material is based upon work supported by the U.S. Department of Energy, Office of Science, National Quantum Information Science Research Centers, Quantum Systems Accelerator. Additional support is acknowledged from the ONR (Grants No. N00014-20-1-2513 and No. N00014-22-1-2280), NSF (PHY-2012068 and the QLCI program through Grant No. OMA-2016245), and European Research Council (ERC) under the European Union's Horizon 2020 research and innovation program (Grant No. 856415). This research was supported in part through the use of University of Delaware HPC Caviness and DARWIN computing systems: DARWIN - A Resource for Computational and Data-intensive Research at the University of Delaware and in the Delaware Region, R. Eigenmann, B. E. Bagozzi, A. Jayaraman, W. Totten, and C. H. Wu, University of Delaware, 2021 [37].

[1] S. M. Brewer, J.-S. Chen, A. M. Hankin, E. R. Clements, C. W. Chou, D. J. Wineland, D. B. Hume, and D. R. Leibrandt, $^{+27}$Al Quantum-Logic Clock with a Systematic Uncertainty below 10^{-18}, Phys. Rev. Lett. **123**, 033201 (2019).

[2] C. Sanner, N. Huntemann, R. Lange, C. Tamm, E. Peik, M. S. Safronova, and S. G. Porsev, Optical clock comparison for Lorentz symmetry testing, Nature (London) **567**, 204 (2019).

[3] T. Bothwell, D. Kedar, E. Oelker, J. M. Robinson, S. L. Bromley, W. L. Tew, J. Ye, and C. J. Kennedy, JILA SrI optical lattice clock with uncertainty of 2.0×10^{-18}, Metrologia **56**, 065004 (2019).

[4] Boulder Atomic Clock Optical Network (BACON) Collaboration, Frequency ratio measurements at 18-digit accuracy using an optical clock network, Nature (London) **591**, 564 (2021).

[5] G. Barontini, L. Blackburn, V. Boyer, F. Butuc-Mayer, X. Calmet, J. R. Crespo López-Urrutia, E. A. Curtis, B. Darquié, J. Dunningham, N. J. Fitch *et al.*, Measuring the stability of fundamental constants with a network of clocks, EPJ Quantum Technol. **9**, 12 (2022).

[6] W. F. McGrew, X. Zhang, R. J. Fasano, S. A. Schäffer, K. Beloy, D. Nicolodi, R. C. Brown, N. Hinkley, G. Milani, M. Schioppo, T. H. Yoon, and A. D. Ludlow, Atomic clock performance enabling geodesy below the centimetre level, Nature (London) **564**, 87 (2018).

[7] M. S. Safronova, D. Budker, D. DeMille, D. F. J. Kimball, A. Derevianko, and C. W. Clark, Search for new physics with atoms and molecules, Rev. Mod. Phys. **90**, 025008 (2018).

[8] D. Antypas, A. Banerjee, C. Bartram, M. Baryakhtar, J. Betz, J. J. Bollinger, C. Boutan, D. Bowring, D. Budker, D. Carney *et al.*, New horizons: Scalar and vector ultralight dark matter, arXiv:2203.14915.

[9] O. Buchmueller, D. Carney, T. Cecil, J. Ellis, R. F. G. Ruiz, A. A. Geraci, D. Hanneke, J. Hogan, N. R. Hutzler, A. Jayich, S. Kolkowitz, G. W. Morley, H. Muller, Z. Pagel, C. Panda, and M. S. Safronova, Snowmass 2021: Quantum sensors for HEP science – interferometers, mechanics, traps, and clocks, arXiv:2203.07250.

[10] M. Takamoto, F.-L. Hong, R. Higashi, and H. Katori, An optical lattice clock, Nature (London) **435**, 321 (2005).

[11] N. D. Lemke, A. D. Ludlow, Z. W. Barber, T. M. Fortier, S. A. Diddams, Y. Jiang, S. R. Jefferts, T. P. Heavner, T. E. Parker, and C. W. Oates, Spin-1/2 Optical Lattice Clock, Phys. Rev. Lett. **103**, 063001 (2009).

[12] P. J. Winzer, D. T. Neilson, and A. R. Chraplyvy, Fiber-optic transmission and networking: the previous 20 and the next 20 years [Invited], Opt. Express **26**, 24190 (2018).

[13] S. Eustice, K. Cassella, and D. Stamper-Kurn, Laser cooling of transition-metal atoms, Phys. Rev. A **102**, 053327 (2020).

[14] A. W. Young, W. J. Eckner, W. R. Milner, D. Kedar, M. A. Norcia, E. Oelker, N. Schine, J. Ye, and A. M. Kaufman, Half-minute-scale atomic coherence and high relative stability in a tweezer clock, Nature (London) **588**, 408 (2020).

[15] M. S. Safronova, M. G. Kozlov, W. R. Johnson, and D. Jiang, Development of a configuration-interaction plus all-order method for atomic calculations, Phys. Rev. A **80**, 012516 (2009).

[16] E. B. Norrgard, D. S. Barker, S. P. Eckel, S. G. Porsev, C. Cheung, M. G. Kozlov, I. I. Tupitsyn, and M. S. Safronova, Laser spectroscopy of the $y\,^7P^o_J$ states of Cr I, Phys. Rev. A **105**, 032812 (2022).

[17] C. Cheung, M. Safronova, and S. Porsev, Scalable codes for precision calculations of properties of complex atomic systems, Symmetry **13**, 621 (2021).

[18] See Supplemental Material at http://link.aps.org/supplemental/10.1103/PhysRevA.107.L051102 for the details of our calculations of the atomic structure, Rabi frequencies, polarizabilities, and the effects of dipolar interactions.

[19] A. Kramida, Y. Ralchenko, J. Reader, and NIST ASD Team, NIST Standard Reference Database 78, Version 5.10, 2022, https://dx.doi.org/10.18434/T4W30F.

[20] M. Takamoto and H. Katori, Spectroscopy of the $^1S_0$- $^3P_0$ Clock Transition of ^{87}Sr in an Optical Lattice, Phys. Rev. Lett. **91**, 223001 (2003).

[21] M. S. Safronova, S. G. Porsev, U. I. Safronova, M. G. Kozlov, and C. W. Clark, Blackbody-radiation shift in the Sr optical atomic clock, Phys. Rev. A **87**, 012509 (2013).

[22] G. Kestler, K. Ton, D. Filin, M. S. Safronova, and J. T. Barreiro, Magic wavelengths of the Sr ($5s^2\,^1S_0 - 5s5p\,^3P_1$) intercombination transition near the $5s5p\,^3P_1$–$5p^2\,^3P_2$ transition, Phys. Rev. A **105**, 012821 (2022).

[23] A. P. Kulosa, D. Fim, K. H. Zipfel, S. Rühmann, S. Sauer, N. Jha, K. Gibble, W. Ertmer, E. M. Rasel, M. S. Safronova, U. I. Safronova, and S. G. Porsev, Towards a Mg Lattice Clock: Observation of the $^1S_0 - {}^3P_0$ Transition and Determination of the Magic Wavelength, Phys. Rev. Lett. **115**, 240801 (2015).

[24] M. S. Safronova, S. G. Porsev, and C. W. Clark, Ytterbium in Quantum Gases and Atomic Clocks: van der Waals Interactions and Blackbody Shifts, Phys. Rev. Lett. **109**, 230802 (2012).

[25] Z.-M. Tang, Y.-M. Yu, J. Jiang, and C.-Z. Dong, Magic wavelengths for the $6s^2\,^1S_0 - 6s6p\,^3P^o_1$ transition in ytterbium atom, J. Phys. B: At., Mol. Opt. Phys. **51**, 125002 (2018).

[26] A. Yamaguchi, M. S. Safronova, K. Gibble, and H. Katori, Narrow-line Cooling and Determination of the Magic Wavelength of Cd, Phys. Rev. Lett. **123**, 113201 (2019).

[27] A. Golovizin, E. Fedorova, D. Tregubov, D. Sukachev, K. Khabarova, V. Sorokin, and N. Kolachevsky, Inner-shell clock transition in atomic thulium with a small blackbody radiation shift, Nat. Commun. **10**, 1724 (2019).

[28] L. Chomaz, I. Ferrier-Barbut, F. Ferlaino, B. Laburthe-Tolra, B. L. Lev, and T. Pfau, Dipolar physics: A review of experiments with magnetic quantum gases, Rep. Prog. Phys. **86** 026401 (2022).

[29] A. de Paz, A. Chotia, E. Maréchal, P. Pedri, L. Vernac, O. Gorceix, and B. Laburthe-Tolra, Resonant demagnetization of a dipolar Bose-Einstein condensate in a three-dimensional optical lattice, Phys. Rev. A **87**, 051609(R) (2013).

[30] S. L. Campbell, R. B. Hutson, G. E. Marti, A. Goban, N. Darkwah Oppong, R. L. McNally, L. Sonderhouse, J. M. Robinson, W. Zhang, B. J. Bloom, and J. Ye, A Fermi-degenerate three-dimensional optical lattice clock, Science **358**, 90 (2017).

[31] T. Nicholson, S. Campbell, R. Hutson, G. Marti, B. Bloom, R. McNally, W. Zhang, M. Barrett, M. Safronova, G. Strouse, W. Tew, and J. Ye, Systematic evaluation of an atomic clock at 2×10^{-18} total uncertainty, Nat. Commun. **6**, 6896 (2015).

[32] S. G. Porsev, M. S. Safronova, U. I. Safronova, and M. G. Kozlov, Multipolar Polarizabilities and Hyperpolarizabilities in the Sr Optical Lattice Clock, Phys. Rev. Lett. **120**, 063204 (2018).

[33] I. Ushijima, M. Takamoto, and H. Katori, Operational Magic Intensity for Sr Optical Lattice Clocks, Phys. Rev. Lett. **121**, 263202 (2018).

[34] K. Ton, G. Kestler, D. Filin, C. Cheung, P. Schneeweiss, T. Hoinkes, J. Volz, M. S. Safronova, A. Rauschenbeutel, and J. T. Barreiro, State-insensitive trapping of alkaline-earth atoms in a nanofiber-based optical dipole trap, arXiv:2211.04004.

[35] S. G. Porsev and A. Derevianko, Multipolar theory of blackbody radiation shift of atomic energy levels and its implications for optical lattice clocks, Phys. Rev. A **74**, 020502(R) (2006).

[36] C. Lisdat, S. Dörscher, I. Nosske, and U. Sterr, Blackbody radiation shift in strontium lattice clocks revisited, Phys. Rev. Res. **3**, L042036 (2021).

[37] https://udspace.udel.edu/handle/19716/29071 (2021).